SCIENCE CHINA
Chemistry

• ARTICLES •

January 2012 Vol.55 No.1: 145–150
doi: 10.1007/s11426-011-4440-6

Cobalt catalysts supported on silica nanotubes for Fischer–Tropsch synthesis

TANG HuoQiang[1], LIEW KongYong[1,2] & LI JinLin[1*]

[1] *Key Laboratory of Catalysis and Materials Science of the State Ethnic Affairs Commission & Ministry of Education, South-Central University for Nationalities, Wuhan 430074, China*
[2] *Faculty of Industrial Science and Technology, Universiti Malaysia Pahang, Kuantan 26300, Malaysia*

Received March 25, 2011; accepted September 18, 2011; published online October 28, 2011

Silica nanotubes (SNT) have been synthesized using carbon nanotubes (CNT) as a template. Silica-coated carbon nanotubes (SNT-CNT) and SNT were loaded with a cobalt catalyst for use in Fischer–Tropsch synthesis (FTS). The catalysts were prepared by incipient wetness impregnation and characterized by N_2 physisorption, X-ray diffraction (XRD), hydrogen temperature programmed reduction (H_2-TPR) and transmission electron microscopy (TEM). FTS performance was evaluated in a fixed-bed reactor at 493 K and 1.0 MPa. Co/CNT and Co/SNT catalysts showed higher activity than Co/SNT-CNT in FTS because of the smaller cobalt particle size, higher dispersion and stronger reducibility. The results also showed that structure of the support affects the product selectivity in FTS. The synergistic effects of cobalt particle size, catalytic activity and diffusion limitations as a consequence of its small average pore size lead to medium selectivity to C_{5+} hydrocarbons and CH_4 over Co/SNT-CNT. On the other hand, the Co/CNT showed higher CH_4 selectivity and lower C_{5+} selectivity than Co/SNT, due to its smaller average pore size and cobalt particle size.

Fischer–Tropsch synthesis, cobalt catalyst, activity, selectivity, silica nanotubes

1 Introduction

The Fischer–Tropsch synthesis (FTS) is a method for the production of liquid hydrocarbons from synthesis gas (CO and H_2) [1,2]. Cobalt-based FTS catalysts have been widely studied because of their high conversion, high selectivity for heavy hydrocarbons, low water-gas shift activity, and comparatively low price [3]. Many studies of FTS catalysts have been carried out using different preparation methods, cobalt loadings and supports (silica, alumina, magnesia, carbon, etc.). It has been found that the support materials have a crucial effect on the activity of heterogeneous catalysts [4–7]. Reuel *et al*. [8] showed that the support can significantly influence the extent of reduction, morphology, adsorption, activity and selectivity properties of the active phase. In FTS, the catalytic behavior of silica-supported cobalt catalysts was found to depend on the nature of the cobalt species, the cobalt particle size, and the texture of the support [9–13].

In recent years, hollow inorganic nanotubes have attracted considerable attention due to their unique structural characteristics and potential applications in catalysis [14–20]. Wang *et al*. [15] have used needle-like $CaCO_3$ nanoparticles as a template to prepare porous hollow silica nanotubes (SNT), which have a uniform open tubular structure with a large surface area. Mokoena *et al*. [21] have studied SNT as a potential support with metals well-dispersed inside the nanotubes.

As a catalyst support, SNT has many advantages such as resistance to acids or bases, stability at high temperatures in inert or reducing atmospheres, and a wide range of pore

*Corresponding author (email: jinlinli@yahoo.cn)

structures and flexibility, which allows the catalyst properties to be tailored for specific needs. The properties of SNT as a support make it suitable for FTS. The use of hollow inorganic nanotubes (SNT, or silica coated carbon nanotubes (SNT-CNT)) as supports for cobalt catalysts for FTS has not been reported so far. In this work, three different hollow inorganic nanotubes (SNT, SNT-CNT, and CNT) were used as a support for cobalt catalysts, and the activity and hydrocarbon selectivities of these catalysts in FTS were investigated.

2 Experimental

2.1 Catalyst preparation

Raw CNT (Chengdu Organic Chemicals Company, China) was used as a template for the preparation of SNT. The CNT was first treated in nitric acid solution using a modification of a procedure reported in ref. [15]. Briefly, 6 g of raw CNT was added to 300 mL of HNO_3 (68 wt.%) and refluxed at 413 K for 8 h in an oil bath to open the tips of the tubes. The mixture was filtered and washed with deionized water until the pH reached 7.0, followed by drying at 373 K for 12 h.

1.0 g of treated CNT and 0.06 g of citric acid were added to a mixture of 300 mL of ethanol and 10 mL of water with vigorous stirring. 4.5 mL of tetraethoxysilane (TEOS) and 0.5 mL of 3-aminopropyltriethoxysilane were added consecutively to the above solution. After stirring the mixture at room temperature for 120 min, about 18 mL of 14 wt.% $NH_3 \cdot H_2O$ was added and the mixture stirred at room temperature for 30 h. The product was centrifuged and washed three times with alcohol and then three times with double-distilled water to remove possible remnants. SNT-CNT was obtained as a black solid and dried at 353 K for 12 h. Finally, the product was heated in air from room temperature to 823 K in a well-controlled tube furnace with a heating rate of 2 K min^{-1} and kept at 823 K for 6 h to obtain SNT.

The CNT, SNT-CNT and SNT calcined in N_2 at 823 K for 6 h were impregnated with the appropriate amount of an ethanol solution of $Co(NO_3)_2 \cdot 6H_2O$ by incipient wetness. The samples were dried at 323 K for 12 h and calcined in N_2 at 623 K for 6 h. All catalysts contained 15 wt.% cobalt and are denoted as Co/CNT, Co/SNT-CNT, and Co/SNT, respectively.

2.2 Catalyst characterization

2.2.1 Transmission electron microscopy (TEM)

TEM is the conventional method used to obtain detailed information about the shape, size, and size distribution of metallic particles. The microstructure of the Co material supported on the inorganic nanotubes was observed with a FEI Tecnai $G^2$20 instrument. Samples were prepared by suspending directly in ethanol with ultrasonication. A copper grid covered with perforated carbon was dipped into the ultrasonicated suspension.

2.2.2 Sample porosity

BET surface area, pore volume and pore size distribution were measured by nitrogen physisorption at 77 K using a Quantachrome Autosorb-1-C-MS instrument. Before the measurements, the samples were outgassed at 473 K for at least 6 h. The surface area was obtained using the Brunauer–Emmett–Teller (BET) model for adsorption data in the relative pressure range from 0.05 to 0.30. The total pore volume was determined from the aggregation of N_2 vapor adsorbed at a relative pressure of 0.99.

2.2.3 X-ray powder diffraction (XRD)

The X-ray diffraction (XRD) patterns were obtained using a Bruker-D8 powder diffractometer with monochromatized Cu-Kα radiation (λ = 1.54056 Å) operated at 40 kV and 40 mA and collected by a Vantec-1 detector. The average Co_3O_4 crystallite size of the catalysts was calculated using the Scherrer equation.

2.2.4 H_2 temperature programmed reduction (H_2-TPR)

Temperature programmed reduction was performed in a Zeton Altamira AMI-200 unit. The catalysts (ca. 0.05 g) were placed in a U-shape quartz reactor, with a thermocouple for continuous temperature measurement. The sample was first flushed with high purity argon at 423 K for 1 h, and the temperature then decreased to 323 K. An Ar gas stream containing 10% H_2 (30 cm^3 min^{-1}) was switched on and the temperature was raised from 323 to 1073 K at a rate of 10 K min^{-1}. The temperature was held at 1073 K for 30 min. Hydrogen consumption was monitored using a thermal conductivity detector (TCD).

The TPR procedure was performed again on a Quantachrome Autosorb-1-C-MS instrument, and the effluent was simultaneously monitored with an Omnistar 300 quadrupole mass spectrometer.

2.3 Fischer–Tropsch synthesis

Fischer–Tropsch synthesis was performed in a fixed-bed reactor. The catalyst (ca. 0.5 g) was reduced in high purity H_2 with a gas hour space velocity (GHSV) of 4 NL.$h^{-1}g^{-1}$ at atmospheric pressure (NL: normal liter, at 298 K and 101.325 kPa). The reactor temperature was increased from ambient to 373 K at 2 K min^{-1}, followed by increasing to 723 K at 1 K min^{-1} and held for 10 h. Subsequently, the reactor was cooled down to 373 K before switching to syngas (H_2/CO = 2; 4 SL h^{-1} g^{-1}) and the pressure was increased to 1.0 MPa (SL: standard liter, at 273 K and 101.325 kPa). The reactor temperature was increased to 493 K over 14 h.

The reaction was carried out at the final temperature. The products were collected in a hot trap (373 K) and a cold trap (271 K). The effluent product gas was passed through an Agilent Micro GC 3000 gas chromatograph for online analysis. Activity is reported as CO conversion. C_{5+} selectivity was calculated by subtracting the amount of C_1–C_4 hydrocarbons in the product gas mixture from the total mass balance.

3 Results and discussion

3.1 Transmission electron microscopy (TEM)

Figure 1 shows TEM images of the supports and the catalysts. As can be seen, the template CNT has a pore diameter of 8–15 nm (Figure 1(a)). The SNT-CNT (Figure 1(b)) shows a pore diameter of 4–10 nm with silica coated on the CNT surface. The shape of SNT-CNT was similar to that of CNT, with a uniform tubular hollow structure and opened tips. This demonstrates that CNT serves as a template for the synthesis of SNT. After the template CNT was removed by calcination, the uniform tubular hollow nanostructure (pore diameter 10–20 nm) is clearly visible in the TEM image of the resulting SNT (Figure 1(c)). The SNT inner diameter is about 10–20 nm, and the outer diameter is about 40–70 nm. From the TEM images of CNT, SNT-CNT and SNT, the outer diameters of SNT-CNT and SNT are larger than the pore size of CNT, indicating that silica layers are located outside the CNT walls. Typical TEM images of the cobalt catalysts are shown in Figures 1(d), 1(e) and 1(f). The TEM image of Co/CNT (Figure 1(d)) shows that the cobalt oxide particles are located both inside and outside the CNT nanochannels. Figures 1(e) and (f) show that the cobalt oxide particles are mostly inside the nanochannels of SNT and SNT-CNT.

3.2 Nitrogen physisorption measurements

The BET surface area, pore size and pore volume data for the supports and the catalysts are listed in Table 1. The pore size of SNT-CNT is similar to that of CNT whilst the pore size of SNT is larger than that of CNT. This suggests that the silica is deposited outside the CNT, and is in agreement with the conclusion from the TEM images. After loading with cobalt, the BET surface area of the catalysts decreased significantly due to the blocking of the pores by the deposited cobalt clusters [8].

3.3 X-ray powder diffraction (XRD)

X-ray powder diffraction patterns of the supports and the catalysts are presented in Figure 2. The peaks at 25.5°, 42.7° and 53.6° correspond to the diffraction peaks of carbon nanotubes, and the peaks at 31.4°, 36.9°, 45.2°, 59.5° and 65.5° can be assigned to Co_3O_4. The intensities of the CNT diffraction peaks are lower for the catalysts than for the corresponding CNT and SNT-CNT, which may be due to the decrease in crystallinity of CNT after loading with higher crystallinity Co_3O_4. The Co/CNT catalyst shows weak Co diffraction peaks, indicating that the cobalt species are well dispersed on the CNT surface. In comparison with Co/CNT, the intensities of the diffraction peaks for both Co/SNT-CNT and Co/SNT are higher, and the peaks are narrower, indicating an increase in Co_3O_4 particle size.

3.4 Temperature programmed reduction (TPR)

TPR profiles of the three catalysts and that of the purified CNT are shown in Figure 3. For the Co/SNT catalyst, two

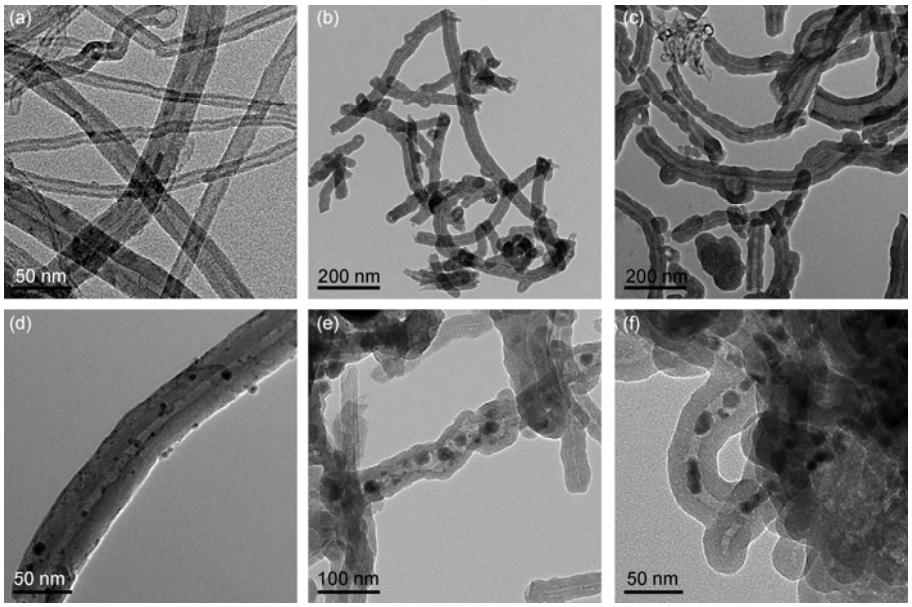

Figure 1 TEM images of CNT (a), SNT-CNT (b), SNT (c), Co/CNT (d), Co/SNT-CNT (e) and Co/SNT (f).

Table 1 BET surface area, pore size, pore volume and Co_3O_4 crystallite size

Sample	S_{BET} (m^2 g^{-1})	Pore volume (cm^3 g^{-1})	Average pore diameter (nm)	Co_3O_4 crystallite diameter (nm) [a)]
CNT	169.1	1.40	11.6	–
SNT	119.2	0.93	16.8	–
SNT-CNT	73.2	0.51	12.0	–
Co/CNT	145.9	1.51	11.8	12.2
Co/SNT	94.7	1.27	17.3	16.6
Co/SNT-CNT	61.9	0.55	12.3	19.8

a) The Co_3O_4 crystallite diameter was calculated using the Scherrer equation.

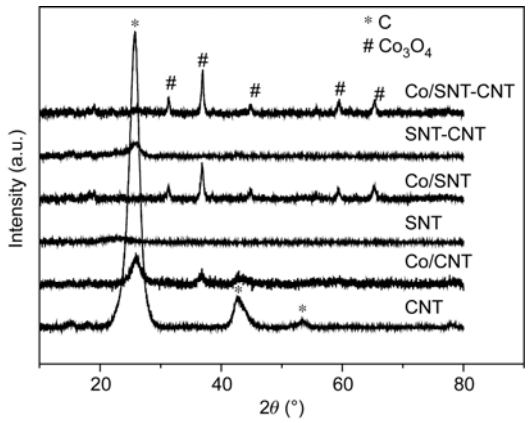

Figure 2 XRD patterns of the supports and the cobalt catalysts.

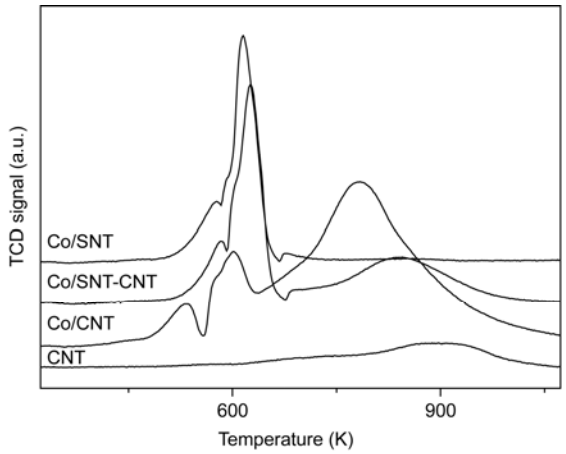

Figure 3 TPR profiles of calcined catalysts and purified CNT.

reduction peaks located at 575 and 614 K are observed and can be attributed to the first reduction step of Co_3O_4 ($Co_3O_4 \rightarrow$ CoO) and the subsequent reduction of the CoO phase ($CoO \rightarrow Co^0$), respectively. The temperatures of both the first and second reduction peaks for SNT-CNT are slightly higher than the corresponding peaks for SNT. The nitrogen physisorption measurements and TEM images both show that the pore size of SNT-CNT is smaller than that of SNT. It can be inferred that Co/SNT catalyst is more easily reduced than the Co/SNT-CNT catalyst due to the larger pore size and lower diffusion limitations of SNT. Studies have suggested that slow diffusional evacuation of the water, which is formed in the reduction, outside the porous structure of catalysts might affect the H_2-TPR profiles by slowing the reduction rate [22]. The peaks at 565 and 790 K for the Co/CNT catalyst can be assigned to the reduction of Co_3O_4 to CoO and the reduction of CoO to Co^0 respectively, while the broad peak appearing at $T > 700$ K results from the gasification of CNT [16]. Its lower reduction temperature shows that the Co/CNT catalyst is more easily reduced than the Co/SNT and Co/SNT-CNT catalysts, which can be attributed to the weaker interaction between cobalt oxide and the carbon support compared to that with the silica support.

Figure 4 shows the TPR-MS profiles of CNT and Co/CNT; the peak intensity of the outlet products was recorded as a function of temperature. When the temperature was increased, no distinct change in CH_4 concentration was observed for CNT (Figure 4(a)). However, for Co/CNT, the CH_4 concentration increased sharply when the temperature was above 600 K, with the maximum value appearing at 850 K (Figure 4(b)), indicating gasification of CNT occurred in the presence of Co. The broad peak at around 785 K in Figure 4 is due to the gasification of CNT, and is strongly overshadowed by the broad tailing of the second TPR peak.

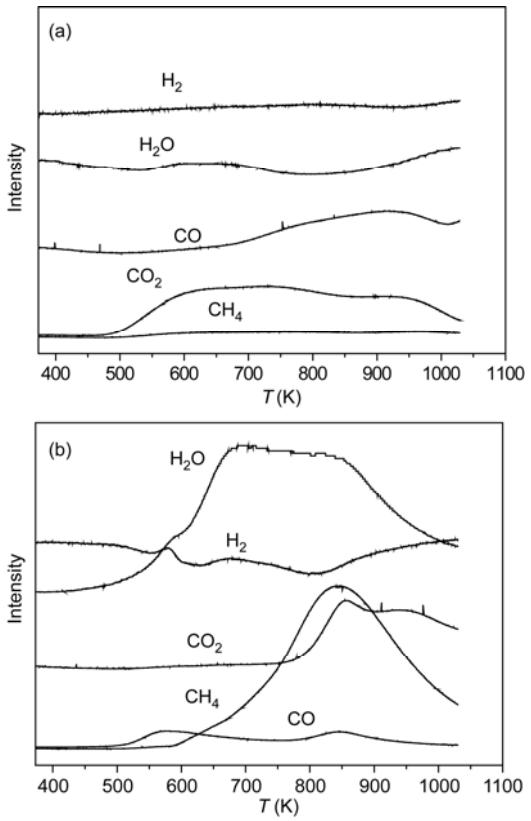

Figure 4 The intensity of products as a function of temperature determined by TPR-MS for CNT (a) and Co/CNT (b).

Table 2 Performance of different catalysts in Fischer–Tropsch synthesis ($H_2/CO = 2$, $P = 1.0$ MPa, $T = 493$ K, GHSV = 4 NL h^{-1} g^{-1})

Catalyst	Cobalt loading (wt.%) [a]	CO conversion (%)	Hydrocarbon selectivity (mol%)				
			CH_4	C_2	C_3	C_4	C_{5+}
Co/SNT	14.87	27.62	5.99	0.57	1.45	1.94	90.04
Co/CNT	14.94	26.94	8.16	0.81	2.58	3.82	84.16
Co/SNT-CNT	15.06	9.88	6.79	0.75	2.28	3.60	86.57

a) The data were determined using inductively-coupled plasma atomic emission spectroscopy (ICP–AES).

3.5 Fischer-Tropsch synthesis

The catalytic performance of the three catalysts in FTS is shown in Table 2. Co/SNT displayed higher activity and higher C_{5+} selectivity than Co/SNT-CNT, while Co/CNT showed similar activity, lower C_{5+} and higher CH_4 selectivity relative to Co/SNT. It can be concluded that the activity and the selectivity of the catalysts are related to the differences in the properties of the supports. It has been suggested that the cobalt catalyst activity for FTS is strongly dependent on cobalt particle size and catalyst reducibility [23,24]. In this work, Co/CNT and Co/SNT displayed higher activity than Co/SNT-CNT due to the higher reducibility and smaller cobalt particle size as shown in the characterization section.

These results also show that the difference in support structure affects the product selectivity in FTS. From Table 2, Co/SNT displayed a high C_{5+} selectivity and low CH_4 selectivity. The difference in selectivity to C_{5+} and CH_4 is due to the effect of the support structure and cobalt particle size [12,25,26]. The larger cobalt particles are more selective for heavier molecular weight hydrocarbons in FTS [27]. This is because dissociative adsorption of CO, which leads to the formation of the $–CH_2–$ fragments required for chain growth, is facilitated on larger cobalt clusters. Although the cobalt particle size in Co/SNT-CNT is the largest of the three catalysts, it shows the lowest activity. It is known that the activity can affect the product selectivity of catalyst in FTS, with lower activity leading to higher CH_4 selectivity and lower C_{5+} hydrocarbon selectivity. On the other hand, diffusion limitations in Co/SNT-CNT, with its smaller average pore size, can also lead to higher CH_4 selectivity and lower C_{5+} hydrocarbon selectivity. The medium selectivity to C_{5+} hydrocarbons and CH_4 of Co/SNT-CNT can therefore be attributed to the synergistic effects of cobalt particle size, catalytic activity and diffusion limitations in Co/SNT-CNT with its small average pore size. The higher CH_4 and lower C_{5+} selectivity of Co/CNT relative to Co/SNT can be attributed to the smaller average pore size and cobalt particle size in the former [27].

4 Conclusions

Various nanotube supports (SNT, SNT-CNT) have been synthesized using CNT as a template. The type of nanotube support (SNT, SNT-CNT and CNT) was found to affect the physicochemical and catalytic properties of cobalt-based catalysts in FTS. Co/CNT and Co/SNT catalysts showed higher activity than Co/SNT-CNT in FTS because of their smaller cobalt particle size, higher cobalt dispersion and stronger reducibility. The difference in support structure also affects the product selectivity of FTS. The synergistic effects of the cobalt particle size, the catalytic activity and the diffusion limitation in Co/SNT-CNT with its small average pore size lead to medium selectivity to C_{5+} hydrocarbons and CH_4 over Co/SNT-CNT. On the other hand, Co/CNT showed higher CH_4 and lower C_{5+} selectivity than Co/SNT, due to its smaller average pore size and cobalt particle size.

This work was supported by the National Natural Science Foundation of China (21073238), the National Basic Research Program of China (2011CB211704) and the Natural Science Foundation of Hubei Province (2009CDA049).

1 Bartholomew CH. Recent developments in Fischer-Tropsch catalysis. *Stud Surf Sci Catal*, 1991, 64: 158–224
2 Dry ME. Fischer–Tropsch reactions and the environment. *Appl Catal A: Gen*, 1999, 189: 185–190
3 Dry ME. The Fischer–Tropsch process: 1950–2000. *Catal Today*, 2002, 71: 227–241
4 Rodriquez-Reinoso F. The role of carbon materials in heterogeneous catalysis. *Carbon*, 1998, 36: 159–175
5 Van Steen E, Prinsloo FF. Comparison of preparation methods for carbon nanotubes supported iron Fischer–Tropsch catalysts. *Catal Today*, 2002, 71: 327–334
6 Hoogenraad MS, van Leeuwarden RAGMM, van Breda-Vriesman GJB, Broersma A, Van Dillen AJ, Geus JW. Metal catalysts supported on a novel carbon support. *Stud Surf Sci Catal*, 1995, 91: 263–271
7 Serp P, Corrias M, Kalck P. Carbon nanotubes and nanofibers in catalysis. *Appl Catal A: Gen*, 2003, 253: 337–358
8 Reuel RC, Bartholomew CH. Effects of support and dispersion on the CO hydrogenation activity/selectivity properties of cobalt. *J Catal,* 1984, 85: 78–88
9 Khodakov AY, Constant AG, Bechara R, Zholobenko VL. Pore size effects in Fischer–Tropsch synthesis over cobalt-supported mesoporous silicas. *J Catal*, 2002, 206: 230–241
10 Borg Ø, Spjelkavik AI, Tveten E, Walmsley JC, Diplas S, Eri S, Holmen S, Rytter E. Fischer–Tropsch synthesis: Cobalt particle size and support effects on intrinsic activity and product distribution. *J Catal*, 2008, 259: 161–164
11 Jacobs G, Das TK, Zhang YQ, Li JL, Racoillet G, Davis BH. Fischer–Tropsch synthesis: Support, loading, and promoter effects on the reducibility of cobalt catalysts. *Appl Catal A: Gen*, 2002, 233: 263–281
12 Iglesia E, Soled SL, Fiato RA. Fischer–Tropsch synthesis on cobalt and ruthenium. Metal dispersion and support effects on reaction rate and selectivity. *J Catal*, 1992, 137: 212–224

13 Iglesia E, Soled SL, Fiato RA. Bimetallic synergy in cobalt–ruthenium Fischer–Tropsch synthesis catalysts. *J Catal*, 1993, 143: 345–368
14 Barrientos-Ramírez S, Ramos-Fernández. EV, Silvestre-Albero J, Sepúlveda-Escribano A, Pastor-Blas MM, González-Montiel A. Use of nanotubes of natural halloysite as catalyst support in the atom transfer radical polymerization of methyl methacrylate. *Micropor Mesopor Mater*, 2009, 120: 132–140
15 Wang JX, Wen LX, Wang ZH, Wang M, Shao L, Chen JF. Facile synthesis of hollow silica nanotubes and their application as supports for immobilization of silver nanoparticles. *Scripta Mater*, 2004, 51: 1035–1039
16 Trepanier M, Tavasoli A, Dalai AK, Abatzoglou N. Co, Ru and K loadings effects on the activity and selectivity of carbon nanotubes supported cobalt catalyst in Fischer–Tropsch synthesis. *Appl Catal A: Gen*, 2009, 353: 193–202
17 Chen W, Fan ZL, Pan XL, Bao XH. Effect of confinement in carbon nanotubes on the activity of Fischer–Tropsch iron catalyst. *J Am Chem Soc*, 2008, 130: 9414–9419
18 Zhang QH, Kang JC, Wang Y. Development of novel catalysts for Fischer–Tropsch synthesis: Tuning the product selectivity. *ChemCatChem*, 2010, 2:1030–1058
19 Kang JC, Zhang SL, Zhang QH, Wang Y. Ruthenium nanoparticles supported on carbon nanotubes as efficient catalysts for selective conversion of synthesis gas to diesel fuel. *Angew Chem Int Ed*, 2009, 48: 2565–2568
20 Wang CF, Pan XL, Bao XH, Direct production of light olefins from syngas over a carbon nanotube confined iron catalyst. *Chin Sci Bull*, 2010, 55: 1117–1119
21 Mokoena EM. Synthesis and use of silica materials as supports for the Fischer-Tropsch reaction. Dissertation for Doctoral Degree. Johannesburg: Faculty of Science, University of the Witwatersrand, 2005
22 Prieto G, Martinez A, Murciano R, Arribas MA. Cobalt supported on morphologically tailored SBA-15 mesostructures: The impact of pore length on metal dispersion and catalytic activity in the Fischer–Tropsch synthesis. *Appl Catal A: Gen*, 2009, 367: 146–156
23 Borg Ø, Eri S, Blekkan EA, Stosater S, Wigum H, Rytter E, Holmen A. Fischer–Tropsch synthesis over γ-alumina-supported cobalt catalysts: Effect of support variables. *J Catal*, 2007, 248: 89–100
24 Belambe AR, Oukaci R, Goodwin Jr JG. Effect of pretreatment on the activity of a Ru-promoted Co/Al_2O_3 Fischer–Tropsch catalyst. *J Catal*, 1997, 166: 8–15
25 Aaserud C, Hilmen AM, Bergene E, Eri S, Schanke D, Holmen A. Hydrogenation of propene on cobalt Fischer–Tropsch catalysts. *Catal Lett*, 2004, 94: 171–176
26 Trepanier M, Dalai A-K, Abatzoglou N. Synthesis of CNT-supported cobalt nanoparticle size on reducibility, activity and selectivity in Fischer–Tropsch reactions. *Appl Catal A: Gen*, 2010, 374: 79–86
27 Lapszewicz JA, Loeh HJ, Chipperfield JR. The effect of catalyst porosity on methane selectivity in the Fischer–Tropsch reaction. *J Chem Soc, Chem Commun*, 1993, 11: 913–914